AGU PUBLICATIONS

JGR

Journal of Geophysical Research: Atmospheres

RESEARCH ARTICLE
10.1002/2015JD024217

Key Points:
- Effect of NO_x descent and SPEs on stratospheric ozone is studied using a chemistry transport model
- In early 2012, intensified descent after SSW leads to more NH stratospheric ozone loss than SPEs
- Model includes improved parameterization of NO_y upper boundary and SPE-driven ion chemistry

Correspondence to:
S.-M. Päivärinta,
sanna-mari.paivarinta@fmi.fi

Citation:
Päivärinta, S.-M., P. T. Verronen, B. Funke, A. Gardini, A. Seppälä, and M. E. Andersson (2016), Transport versus energetic particle precipitation: Northern polar stratospheric NO_x and ozone in January–March 2012, *J. Geophys. Res. Atmos.*, *121*, 6085–6100, doi:10.1002/2015JD024217.

Received 11 SEP 2015
Accepted 13 APR 2016
Accepted article online 3 MAY 2016
Published online 25 MAY 2016

Transport versus energetic particle precipitation: Northern polar stratospheric NO_x and ozone in January–March 2012

S.-M. Päivärinta[1,2], P. T. Verronen[1], B. Funke[3], A. Gardini[3], A. Seppälä[1], and M. E. Andersson[1]

[1]Earth Observation, Finnish Meteorological Institute, Helsinki, Finland, [2]Department of Physics, University of Helsinki, Helsinki, Finland, [3]Instituto de Astrofísica de Andalucía, CSIC, Granada, Spain

Abstract In early 2012, a strong sudden stratospheric warming (SSW) took place, accompanied by several medium-scale solar proton events (SPEs). Here we use a chemistry transport model (CTM) in order to assess the relative contributions of (1) intensified downward transport of odd nitrogen (NO_x) and (2) in situ production of NO_x by protons, on stratospheric NO_x and ozone during January–March 2012. The CTM is constrained by an upper boundary condition for reactive nitrogen (NO_y) species, based on satellite observations from Michelson Interferometer for Passive Atmospheric Sounding (MIPAS) on board Envisat, and includes a new parameterization of the SPE-caused effects on NO_y and odd hydrogen (HO_x) species. We found that the amount of NO_x increases due to both transport and in situ production effects, the intensified descent of NO_x dominating the middle and upper stratospheric impact. The model results indicate NO_x enhancements of 120–3300% (5–48 ppbv) between 38 and 50 km, caused by the transport of mesosphere/lower thermosphere NO_x down to the stratosphere following the SSW. The SPEs increase NO_x by up to 820–1200% (14–21 ppbv) at 33 to 50 km. The effect on the stratospheric ozone is larger following the downward transport of NO_x than during and after the SPEs. The model predicts ozone losses of up to 17% and 9% at around 40 km due to transport and SPE effects, respectively.

1. Introduction

Solar extreme ultraviolet radiation, soft X-rays, and auroral electrons produce odd nitrogen ($NO_x = N + NO + NO_2$) constantly in the upper mesosphere and lower thermosphere [*Barth*, 1992]. In the stratosphere, the main source for NO_x is the oxidation of nitrous oxide (N_2O). The photochemical lifetime of the mesosphere/lower thermosphere (MLT) NO_x ranges from days to months in the absence of solar radiation. During the dark polar winters NO_x can be transported from the MLT region down to the lower stratosphere [e.g., *Solomon et al.*, 1982; *Funke et al.*, 2014a]. In the stratosphere, below about 50 km, NO_x can take part in chemical catalytic cycles destroying ozone [e.g., *Callis et al.*, 1991]. A change in the middle atmospheric ozone balance, in turn, could have an effect on the middle atmospheric dynamics, i.e., temperatures and winds [*Langematz et al.*, 2003; *Lu et al.*, 2008; *Kvissel et al.*, 2012] and in the end, through interaction between atmospheric waves and the mean flow, also on the regional polar climate [*Rozanov et al.*, 2005; *Seppälä et al.*, 2013; *Baumgaertner et al.*, 2011; *Rozanov et al.*, 2012].

Downward transport of NO_x can be first interrupted and then intensified by dynamical events known as sudden stratospheric warmings (SSWs). According to *Andrews et al.* [1987] and *Charlton and Polvani* [2007], major SSW events occur on a quite regular basis taking place on average once every other winter or twice every three winters in the Northern Hemisphere (NH). Note that these are averaged occurrence rates for major SSWs and large variation takes place in the occurrence and that minor SSWs are even more frequent than the major ones. In the Southern Hemisphere (SH), only one SSW event has been observed [*Newman and Nash*, 2005; *Thompson et al.*, 2005]. The hemispherical differences in the SSW occurrence rates arises from the larger planetary wave activity driven by the distribution of seamasses and landmasses in the NH. A sudden warming of the stratosphere, cooling of the mesosphere, and weakening, or even reversal, of the zonal mean zonal wind are all associated with SSWs and are in fact linked to enhanced planetary wave activity and thus enhanced wave damping in the middle atmosphere [*Matsuno*, 1971; *Limpasuvan et al.*, 2012]. During SSW events the polar vortex is either split or displaced from the pole interrupting the downward transport of long-lived tracers

from the MLT region but also simultaneously allowing mixing of polar and midlatitude air masses. Intensified descent of MLT air down to the middle atmosphere takes place after strong SSWs when the stratopause reforms at very high (even about 80 km) altitudes after the recovery of the polar vortex [*Manney et al.*, 2008; *Orsolini et al.*, 2010].

Solar proton events (SPEs) are the most impulsive particle source producing NO_x directly in the middle atmosphere, especially in the stratosphere. SPEs are sporadic but tend to occur more frequently around the solar maximum [*Jackman et al.*, 2009]. During SPEs, protons and heavier ions emitted from the Sun are guided by the Earth's magnetic field to the polar regions where they precipitate into the Earth's atmosphere, simultaneously in both hemispheres. In the atmosphere, energetic particles produce NO_x and also odd hydrogen ($HO_x = H + OH + HO_2$) through dissociation and ionization processes [e.g., *Seppälä et al.*, 2004; *Jackman et al.*, 2005; *López-Puertas et al.*, 2005; *Verronen et al.*, 2005, 2006; *Seppälä et al.*, 2008]. The effects of the SPEs on NO_x are more pronounced in the winter hemisphere where the lower level of solar radiation results in a longer chemical lifetime and thus enables the downward transport. The photochemical lifetime of HO_x is relatively short, and as a result all HO_x driven effects are local, with no further downward transport taking place.

Several previous studies have discussed the separate effects of SPEs and SSWs, accompanied by the enhanced mesosphere-to-stratosphere descent, on the middle and upper atmospheric NO_x and the possible following effects on stratospheric ozone [e.g., *Manney et al.*, 2009; *Jackman et al.*, 2008; *Randall et al.*, 2009; *Funke et al.*, 2011; *Salmi et al.*, 2011]. *Holt et al.* [2013] concluded that the largest stratospheric NO_x increases occur after December to early January SSWs followed by an elevated stratopause. The only situations where NO_x reached stratospheric altitudes and a simultaneous signal on ozone was observed are those that took place in early 2004 [e.g., *Randall et al.*, 2005; *Semeniuk et al.*, 2005] and early 2012 [*Jackman et al.*, 2014; *Päivärinta et al.*, 2013]. The 2004 case started with a SSW already in late December 2003 and was followed by intensified downward transport of NO_x in early January 2004: large amounts of additional MLT NO_x, originally produced in the lower thermosphere due to low energy particle precipitation, was transported down to the stratosphere inside the strong polar vortex reformed after the December SSW [*Clilverd et al.*, 2006, 2009]. The 2012 case started with a later, mid-January SSW, and the enhanced descent of NO_x was accompanied by in situ production of NO_x due to four SPEs during January and March.

Päivärinta et al. [2013] studied the winter/spring of 2012 but could not separate the effects and the relative importance of transport and in situ production on the stratospheric NO_x and ozone levels based only on satellite observations. Here we use the FinROSE chemistry transport model (CTM) together with satellite observations from Michelson Interferometer for Passive Atmospheric Sounding (MIPAS)/Envisat and MLS (Microwave Limb Sounder) on board the Aura satellite in order to assess the separate contributions of (1) intensified NO_x transport after the January 2012 SSW and (2) NO_x in situ production due to the early 2012 SPEs, on stratospheric NO_x, and ozone levels.

2. Modeling

FinROSE is a global three-dimensional chemistry transport model (CTM) designed for middle atmospheric studies (further developed model version of the one described by *Damski et al.* [2007]). The model dynamics (e.g., temperature, horizontal winds, and pressure) are from external sources, i.e., changes in atmospheric composition do not affect the model dynamics. Vertical wind is calculated inside the model by using the continuity equation.

In this study FinROSE is run with 72 vertical levels (about 0–80 km), a horizontal resolution of 5° × 4° (longitude × latitude) and is driven by NASA's MERRA (Modern Era Retrospective-analysis for Research and Applications) data [*Rienecker et al.*, 2011]. The model calculates distributions of 41 species in the stratosphere and MLT region taking into account both chemistry and dynamics. Only the long-lived constituents are transported. The model includes about 120 homogeneous reactions and 30 photodissociation processes. Chemical kinetic data, reaction rate coefficients, and absorption cross sections are taken from look-up-tables based on the Jet Propulsion Laboratory compilation by *Sander et al.* [2006], including updates from the available supplements. Photodissociation frequencies are calculated using a radiative transfer model [*Kylling et al.*, 1997]. In addition to homogeneous chemistry, the model also includes heterogeneous chemistry, i.e., formation and sedimentation of polar stratospheric clouds (PSCs) and reactions on PSCs. Chemistry is not defined in the troposphere, but the tropospheric abundances are given as boundary conditions.

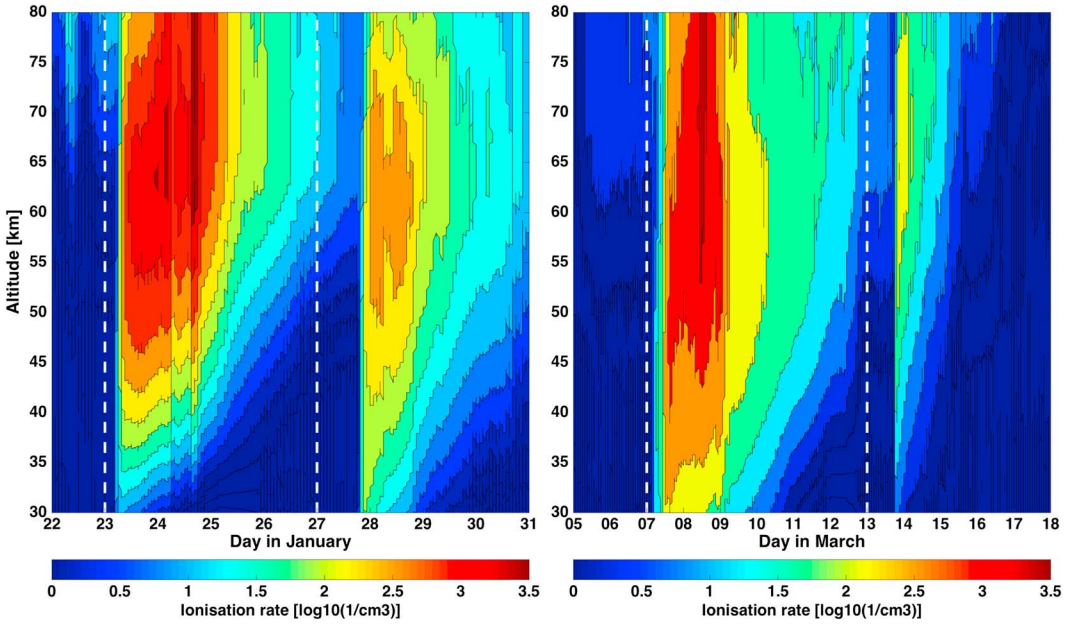

Figure 1. Ionization rates for the January and March 2012 SPEs in the upper stratosphere and mesosphere. White vertical dashed lines indicate the start days of the SPEs.

At the upper boundary, ozone is constrained by the MLS/Aura climatology and NO_y species (HNO_3, NO_2, NO, N_2O_5, and $ClONO_2$) by excess NO_y produced by energetic particle precipitation (EPP). The excess NO_y is derived from MIPAS/Envisat observations, using a tracer correlation method based on MIPAS CH4 and CO observations, and parameterized in terms of *Ap* index and seasonal evolution [*Funke et al.*, 2014a]. The upper boundary condition (UBC) in FinROSE is introduced on a daily basis only on the two upmost levels, at 0.0205 hPa (~75 km) and 0.0075 hPa (~80 km), in every model grid point in the polar areas between 70 and 90°S/N. The UBC is simply the sum of the excess NO_y and the model NO_y, calculated before the implementation of the condition. The purpose of the UBC is to give the model a source for thermospheric NO_y descending from altitudes above the model vertical grid and thus enable the downward transport of NO_x inside the polar vortex, especially following SSWs and elevated stratopause events.

Production of nitric acid (HNO_3) during SPEs has been one of the outstanding problems in understanding the atmospheric effects of EPP [*Jackman et al.*, 2008; *Funke et al.*, 2011]. Models describing atmospheric effects of EPP using the standard parameterization of HO_x and NO_x or ion chemistry too simplified for the lower ionosphere (*D* region) have greatly underestimated the amount of HNO_3 during solar proton events. FinROSE utilizes a new and revised parameterization of ion chemistry which considers the redistribution of NO_y due to negative ion chemistry [*Verronen and Lehmann*, 2013]. This parameterization is based on an ensemble of results from the Sodankylä Ion and Neutral Chemistry model [*Verronen et al.*, 2005], and it consists of a set of so-called P/Q numbers for 10 neutral species: H, OH, HNO_2, HNO_3, $N(^4S)$, $N(^2D)$, NO, NO_2, NO_3, and N_2O_5. The P/Q numbers vary with respect to the species, altitude, ionization rate, solar zenith angle, and season (through atmospheric conditions). They are used to calculate the rate of change (molecules cm^{-3} s^{-1}) for the neutral species, simply by multiplying them by the particle ionization rate. Ionization rates, in turn, are calculated using GOES 11 satellite proton flux data (available from, e.g., the NOAA National Geophysical Data Center World Wide Web server, www.ngdc.noaa.gov/stp/stp.html). GOES observations are converted to differential flux spectra, and ionization rates for every model time step, i.e., every 30 min, are then calculated using the empirical energy range relation of protons (for details, see *Verronen et al.* [2005, and references therein]). Ionization rates used in the model are presented in Figure 1.

The early 2012 SPEs in January and March were comparable with the medium scale January 2005 event with maximum proton fluxes of >6000 pfu (particles flux unit, particles cm^{-2} s^{-1} sr^{-1}). The proton fluxes during the first events both in January and in March were elevated for nine consecutive days before returning back to pre-SPE levels. More information on the 2012 SPEs is given in Table 1 and in, e.g., *Jackman et al.* [2014].

Table 1. Timings and Magnitudes of the Early 2012 SPEs[a]

	Start (Day/Month)	Peak (>10 MeV) (Day/Month)	Proton Flux (pfu)
SPE1	23/01	24/01	6310
SPE2	27/01	28/01	796
SPE3	07/03	08/03	6530
SPE4	13/03	13/03	469

[a]The four cases of SPEs indicate the different events that took place in January (SPE1 and SPE2) and March (SPE3 and SPE4).

In the text, we will refer to the January SPEs as SPE1 (first event) and SPE2 (second event) and to the March events as SPE3 (first) and SPE4 (second).

We use the World Meteorological Organization and *Charlton and Polvani* [2007] definition for major SSWs: (1) zonal mean zonal wind reversal at 10 hPa at 60°N and (2) positive temperature gradient at 10 hPa between 60 and 90°N. If only the second criterium is fulfilled, the SSW is classified as a minor SSW. According to this definition the central date for the 2012 SSW was 14 January 2012, and the warming can be classified as a strong minor SSW. The warming was followed by an elevated stratopause and intensified downward transport of MLT air. The event affected the dynamics and composition of all the middle atmosphere altitudes between 30 and 95 km. The meteorological background conditions have been discussed in more detail by *Päivärinta et al.* [2013].

We conducted four FinROSE simulations for the period of January–April 2012: (1) a control run, (2) an SPE run, (3) a UBC run, and (4) an all-encompassing run (UBC + SPE). Runs 1 and 2 were started from the same initial conditions obtained from a 10 year control run (2002–2012) with no UBC implemented for the NO_y species. Runs 3 and 4 were also started from the same initial conditions but now based on a 10 year run (2002–2012) with the UBC for NO_y implemented. Note that due to the different initial conditions of the model runs, the total effect in run 4 is not exactly the sum of runs 2 and 3 (although the difference is small).

We first, in section 4, analyze the overall behavior of FinROSE during early 2012 by contrasting the model NO_x, HNO_3, and O_3 against satellite observations from MIPAS and MLS, focusing on the SSW and SPE periods. To do this, MIPAS/Envisat and MLS/Aura averaging kernels (AKs) have been applied to the model NO_x and HNO_3 results, respectively, in order to make them comparable to the observations by eliminating issues related to the different vertical resolutions of the model and observations. For NO_x, we also show results without AKs in order to show the effect of the kernels on the agreement between the model and observations. AKs have not been applied to the FinROSE ozone results due to the very minor effect they had. For the comparison purposes we use measurements between 70 and 90°N, and model results colocated with the observation times and geolocations.

Then, in section 5, we assess the relative contributions of the intensified downward transport and the January/March SPEs on stratospheric NO_x and O_3 by comparing runs 2, 3, and 4 to the control run. In contrast to the model-measurement comparisons in section 4, where measurement AKs were applied to model results, this part of the analysis uses true polar averages (70–90°N) calculated from the "as is" model results (no AKs applied).

3. Satellite Observations

3.1. MIPAS/Envisat

MIPAS NO and NO_2 observations taken in the nominal observation mode [*Funke et al.*, 2014b] have been used to evaluate the modeled NO_x response. We use L2b version of NO (V5r_NO_221) and NO2 (V5r_NO2_221) provided by the Karlsruhe Institute of Technology/Instituto de Astrofísica de Andalucía research data processor [*von Clarmann et al.*, 2013]. In the middle- to high-latitude polar winters, typical vertical resolutions are 4–6 km in the stratosphere and 6–9 km in the mesosphere, while the single-profile precision is on the order of 5–15%. Systematic errors, dominated by non-LTE-related uncertainties, have been estimated to be less than 10%. Meaningful data are obtained in polar winters up to 70 km.

MIPAS O_3 observations (V5r_O3_225) were also taken in the nominal mode [*von Clarmann et al.*, 2013]. The single measurement precision ranges from 0.1 ppmv around the stratopause to 0.25 ppbv above and below. Vertical resolution is 3–4 km below 1 hPa and 5–7 km above. Meaningful data are obtained in the whole vertical range of interest (25–70 km).

3.2. MLS/Aura

We use observations from the MLS instrument on board the Aura satellite [*Waters et al.*, 2006] in order to study the HNO_3 response on the early 2012 SPEs. We utilize Version 4.2 Level 2 daily mean HNO_3 data for the whole period of interest and for the latitudinal band of 70–82.5° in the NH. The data were screened according to the MLS data description and quality document [*Livesey et al.*, 2015]. The recommended altitude range for MLS HNO_3 data is normally 40–45 km (2.15–1.5 hPa) [*Santee et al.*, 2007; *Livesey et al.*, 2015]. During large SPEs, however, significant HNO_3 enhancements in the upper stratosphere and lower mesosphere improve the signal-to-noise ratio of the observations. In fact, *Verronen et al.* [2011] have shown that it is possible to use the data to study SPE-related changes up to about 70 km (0.046 hPa). For this data, the standard error of the mean varies between 10 and 60% for the SPEs in January and early March above 45 km, i.e., in the region where the HNO_3 enhancements due to particle precipitation mainly takes place. For the mid-March SPE, the standard error of the mean (SEM) increases up to more than 600%, indicating worsening of the signal-to-noise ratio. The vertical resolution of HNO_3 above 30 km (10 hPa) varies between 3 and 5 km. Note that we only use MLS nighttime (solar zenith angle >100°) observations in our study.

4. Model-Measurement Comparison

Figure 2 shows the distribution of January to early April NO_x from MIPAS and FinROSE (SPE and UBC both applied, i.e., run 4) with (bottom row) and without (top row) AKs being applied to the model results and also the relative difference between them (FinROSE-MIPAS). The agreement between MIPAS and FinROSE is reasonably good: the timing of the descent, starting few days after the mid-January SSW, and the altitudes affected by the descent (~30–75 km) show very similar features, both in the observations and in the model results, both with and without the AKs. In fact, the 10 ppbv NO_x isolines of MIPAS and FinROSE agree well during the whole period from the mid-January SSW to early April.

From early to mid-January the model (AKs applied) shows enhanced amounts of NO_x (8–30 ppbv) between 37 and 65 km, not detected in the observations, leading up to 250% differences between the simulated and observed NO_x. Also, during the period of intensified descent, following the mid-January SSW, there is a model overestimation by up to 135% in the same altitude region. When strong in situ NO_x production occurs due the January SPEs, there is a better agreement between the model and observations. In the stratosphere, below about 40 km, FinROSE suggests up to 70% lower NO_x amounts than observed by MIPAS. Note that all the above differences are larger when AKs are not applied to FinROSE results. Above 65 km, the model without AKs overestimates NO_x before the mid-January SSW, whereas with AKs there is an underestimation by up to 60%.

The model underestimation below 40 km (Figure 2, bottom row, AKs applied) is related to a rather low NO_x background in FinROSE. This has been seen, for example, during multimodel-measurement comparisons (i.e., the so-called HEPPA2 project, not shown). The underestimation above 65 km is caused by two things:

1. The application of AKs in the case of NO is tricky because the NO retrieval response in the mesosphere is affected by the thermospheric column. In other words, the MIPAS AKs would work better if applied to the full NO profile (0–200 km). FinROSE (as many other models), however, has no thermosphere included.
2. The UBC used in the model runs is the parameterized MIPAS excess NO_y (not the observed one). The parameterization does neither account for dynamical intra-annual variability (not a big issue in 2012) nor for SPEs (an issue in 2012).

An important factor strongly affecting the model results and the simulated downward transport of NO_x is the meteorological data (see section 2) used in the model. When comparing temperature profiles between the observations and model (Figure 3), it is clear that the reanalysis temperatures are 5–25 K (4–14%) higher above 60 km than the MIPAS observations. This results in stronger downward transport of MLT air to the middle atmosphere in the simulations using the reanalysis data, explaining at least partly the larger NO_x abundances in the lower mesosphere after the SSW. Also, some features in early 2012, especially the elevated stratopause

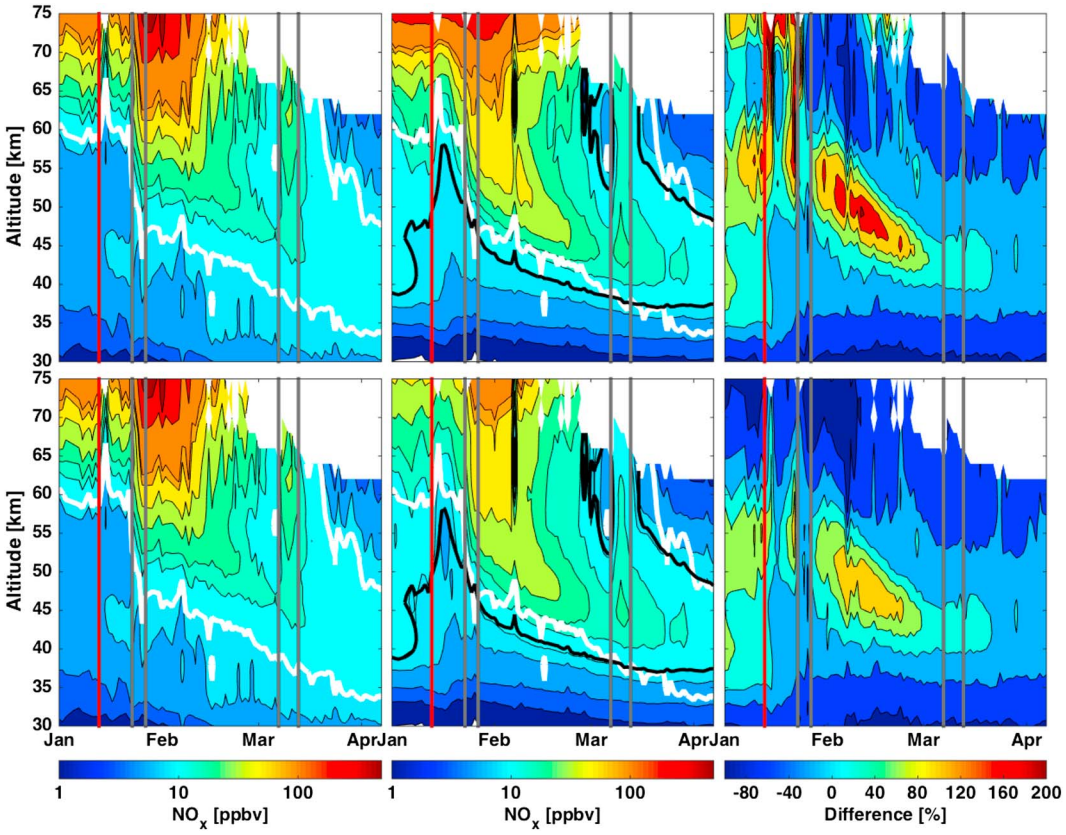

Figure 2. January to early April NO_x (ppbv) between 30 and 75 km from (left column) MIPAS and (middle column) FinROSE-CTM (UBC and SPE both applied) (top row) without and (bottom row) with averaging kernels being applied to the model results. (right column) The difference (%) between FinROSE and MIPAS. The overlaid contours are values of 1, 3, 5, 8, 10, 15, 20, 30, 50, 80, 100, 250, 500 ppbv and −100, −60, −20, 20, 60, 100, 150, 200% for the absolute values and difference, respectively. The white contour in Figure 2 (left and middle columns) denotes the MIPAS and the bold black contour in Figure 2 (middle column) the FinROSE 10 ppbv isoline for NO_x. The vertical red line shows the time point of the SSW and the vertical gray lines the time points of the SPEs.

after the SSW, are not perfectly prescribed since the UBC parameterization does not account for interannual dynamical variability.

In addition to the UBC, another factor strongly affecting the modeled NO_x is the parameterization of its production during the January and March SPEs. It is clear from Figure 2 that there is good agreement in timing of the SPEs between the simulation (with and without AKs) and observations. MIPAS shows that NO_x amounts increase substantially during the SPEs, and FinROSE is able to reproduce these enhancements reasonably well. For example, at 60 km SPE1 increases MIPAS NO_x by about 70 ppbv, while FinROSE underestimates the production by 28%, with AKs applied. Note that if AKs are not applied, the underestimation is less than 3%. Similarly, the NO_x production by SPE3 is underestimated, e.g., by 10–15 ppbv at 60 km.

Figure 4 shows time series of the observed and modeled (AKs applied) NO_x in the upper stratosphere (46 km) and lower mesosphere (60 km). In addition to the all-encompassing model run discussed earlier in this section, we also present model results from the control run (no SPEs or UBC for NO_x included), SPE run (only SPEs included) and UBC run (only UBC included). It is clear that by introducing the NO_y UBC to the model, the agreement between the observations and model improves drastically both in the upper stratosphere and lower mesosphere. By including only the effect of the SPEs, the model behavior in the upper stratosphere improves only during SPE1 and SPE2, but becomes worse after mid-February when the MLT NO_x, not included in the model in this model run, descends lower in the atmosphere. In the lower mesosphere, the SPE run underestimates the amount of NO_x throughout the period from January to early March. Due to the meteorological data and the too strong NO_x descent in the model, the all-encompassing run overestimates the amount of

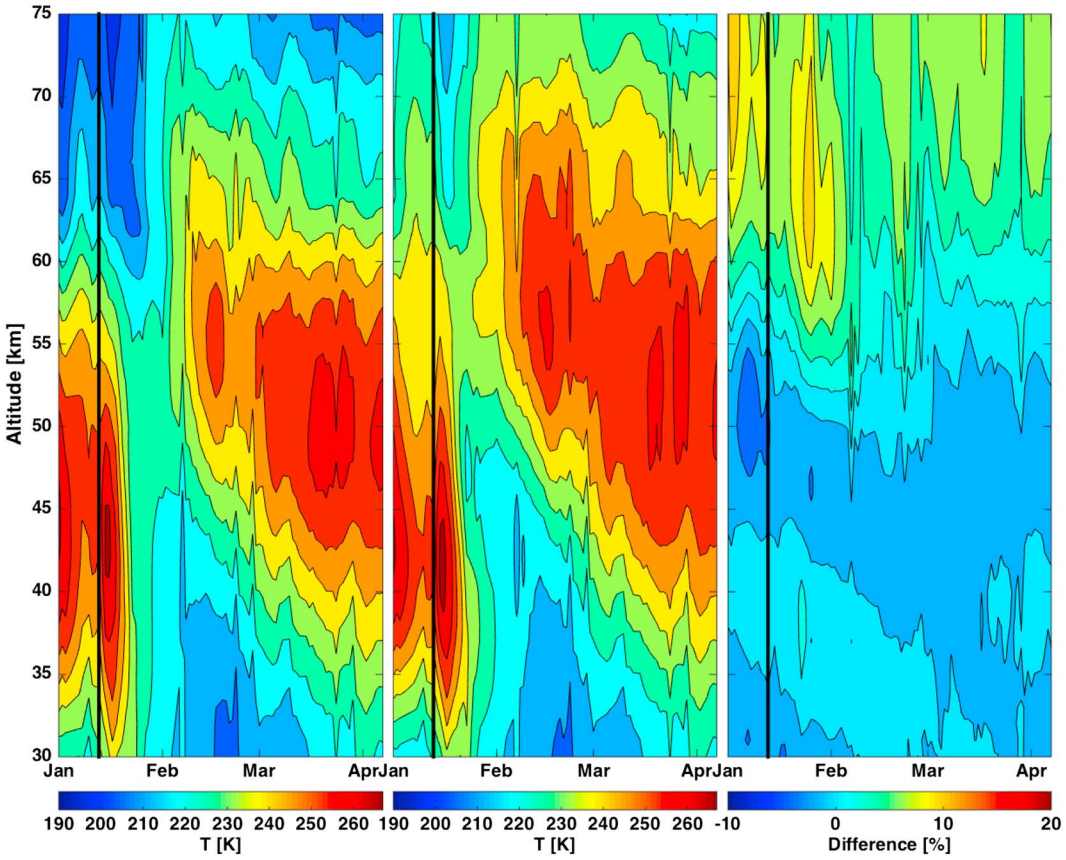

Figure 3. January to early April temperatures (K) between 30 and 75 km from (left) MIPAS and (middle) FinROSE-CTM with averaging kernels being applied to the model results. (right) The difference (%) between the observations and the CTM. The overlaid contours are values of 190–267 K with 7 K level step and −10–20% with 2% level step for the absolute values and difference, respectively. The vertical black line shows the time point of the SSW.

NO_x in the upper stratosphere, as discussed earlier in this section. The agreement between the observations and model is worst when no UBC or SPE parameterization is included in the model.

Figure 5 shows HNO_3 in early 2012 from the middle stratosphere to upper mesosphere as observed by MLS and simulated by the model (all-encompassing run 4). The background level of HNO_3 above 40 km is very similar in both (<1 ppbv), as well as the stratospheric HNO_3 maximum below 40 km (<4–5 ppbv). SPE1 increases HNO_3 by <3 ppbv between 45 and 75 km according to the observations, but even up to 6 ppbv in the simulation. This indicates more than 100% overestimation by the model during a time period when MLS measurement error is not more than about 20%. During SPE2 and SPE3, the agreement is reasonable with only 20–40% difference between 55 and 65 km, fitting inside the MLS measurement error limits of 20–100%. The overall effects extend from 45 to 70 km with HNO_3 increases up to ~2 ppbv both in MLS and in FinROSE. MLS shows, however, a rapid return of the HNO_3 back to the background levels above about 53 km 2 days after SPE3 and then again an increase back to the enhanced levels. This double peak structure is not captured by the model simulations and leads to an overestimation of about 1 ppbv followed by an underestimation of <3 ppbv. The model behavior reflects the SPE ionisation rates which start to decrease after 9 March and continue doing so until the next event on 13 March (see Figure 1). Also, the measurement error of MLS observations during this time period increases rapidly up to more than 600%, indicating a large uncertainty in the observations. SPE4 did not have a significant effect on HNO_3: according to the observations, only an increase of about 1 ppbv took place between 45 and 56 km, but this was not as clearly linked to the SPEs as the previous events, and the uncertainty of the observations was of the same magnitude as those following SPE3. In the model, SPE4 appears to have no effect on the HNO_3.

Figure 6 shows the ozone comparison between MIPAS and FinROSE (all-encompassing run 4). The overall distribution of ozone is more or less similar in the model and in the observations. The largest differences arise

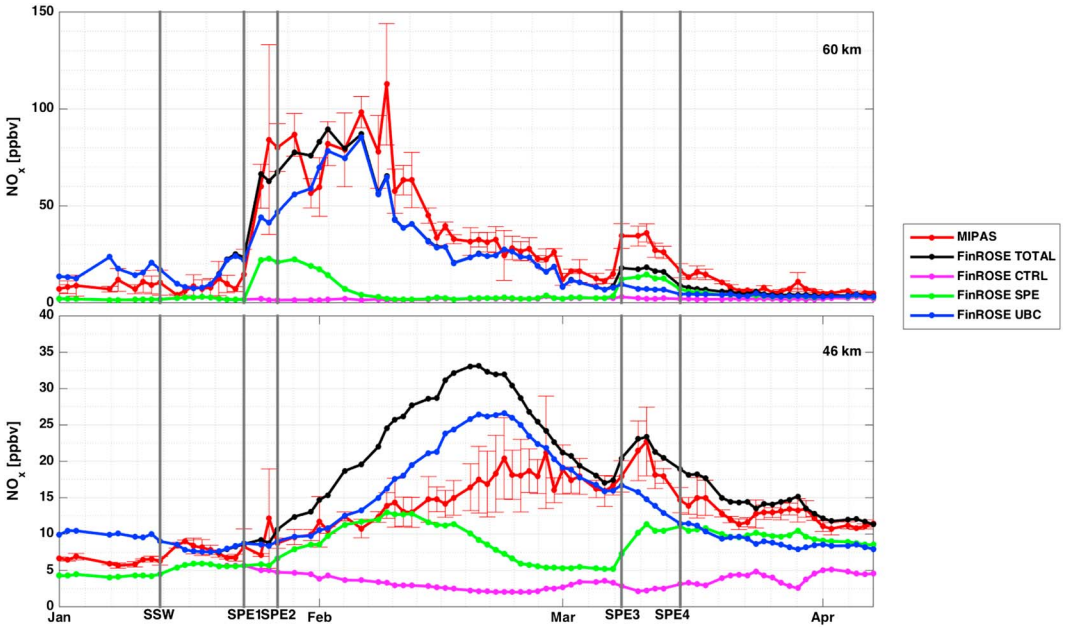

Figure 4. NO_x (ppbv) time series during January to early April in the lower mesosphere (top, 60 km) and the upper stratosphere (bottom, 46 km) as observed by MIPAS (red) and simulated by FinROSE-CTM (averaging kernels applied). All model runs are included in the figure: (1) control (magenta) run, (2) SPE (green) run, (3) UBC (blue) run, and (4) all-encompassing (black) run. MIPAS measuring errors (2*SEM) are plotted as error bars together with the observations. The vertical dark gray lines indicate the time points of the SSW and SPEs.

from the location of the stratospheric ozone layer (situated about 5 km lower in the middle atmosphere in FinROSE) and the mesospheric ozone amounts (generally about 70% lower in FinROSE). As mentioned above, the model/reanalysis temperature close to the stratopause is higher than observed. According to *Sofieva et al.* [2012], temperature and ozone are anticorrelated in the mesosphere and also in the upper stratosphere [e.g., *Smith*, 1995; *Smith et al.*, 2009; *Damiani et al.*, 2010]. In this case, the too low ozone values in the model mesosphere could thus be partly explained by the too high temperatures in the same region, but also due

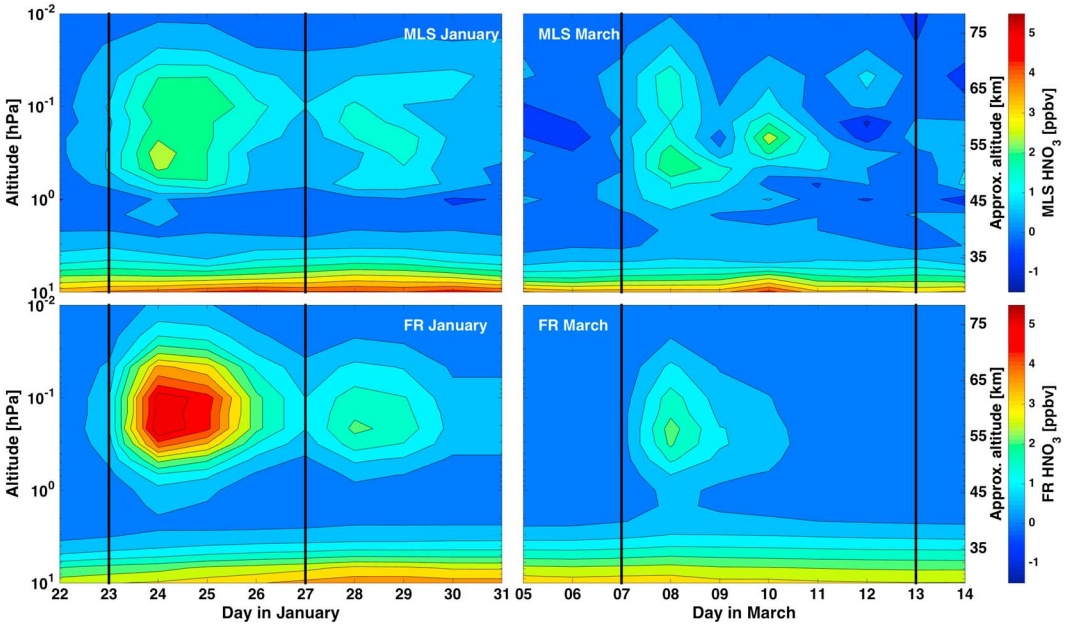

Figure 5. HNO_3 (ppbv) between 30 and 75 km from (top row) MLS and (bottom row) FinROSE-CTM (UBC and SPE both applied) for the (left column) January and (right column) March SPEs.

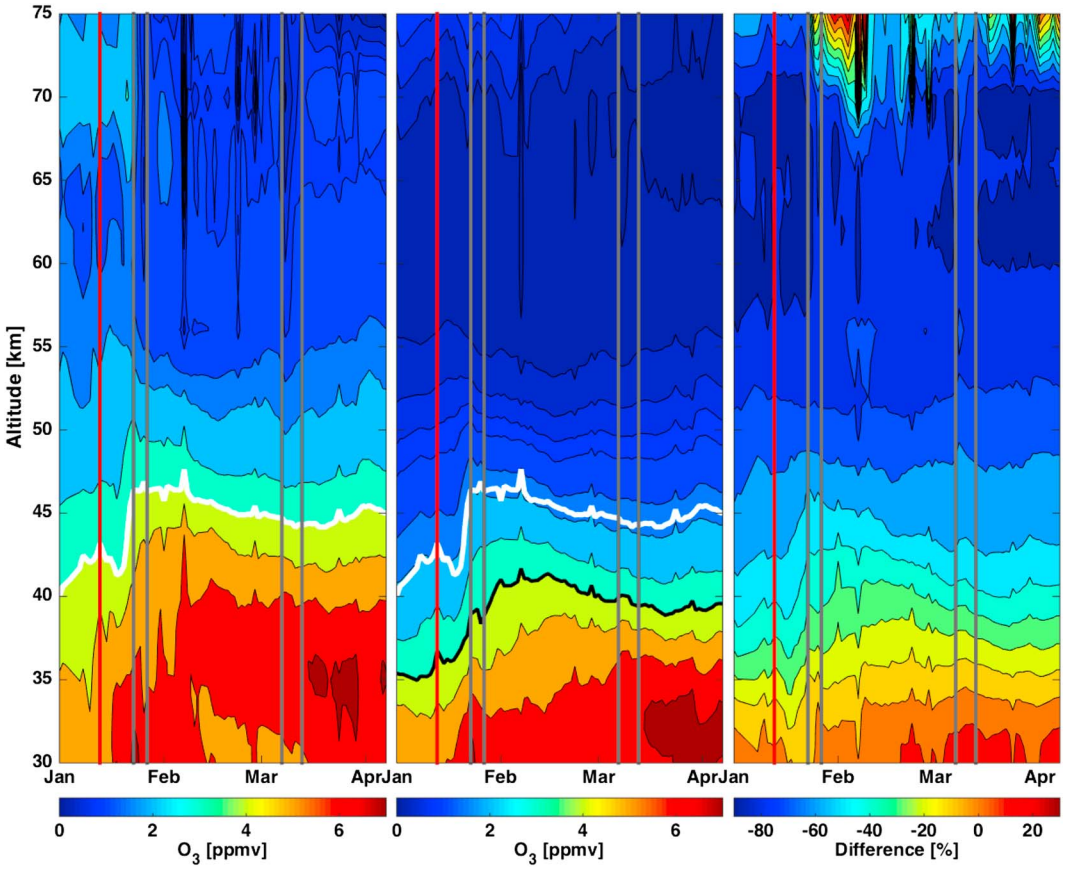

Figure 6. Same as Figure 2, but for ozone and without AKs. Here the overlaid contours are values of 0, 0.2, 0.4, 0.6, 0.8, 1, 1.5, 2, 3, 4, 5, 6, 7 ppmv and −90, −80, −70, −60, −50, −40, −30, −20,−10, 0, 10, 20, 30% for the absolute values and difference, respectively. (left and middle) The white contour denotes the MIPAS and the bold black contour in Figure 6 (middle) the FinROSE 4 ppmv isoline for O_3.

to the vicinity of the upper boundary and thus the possible lack of some MLT processes that would completely describe ozone in this region. On the other hand, the temperature comparison in Figure 3 indicates significant dynamical biases in the model relative to observations. This may be another reason for the ozone differences. A smaller part of the mesospheric differences can also be explained by the positive bias of MIPAS ozone observations [*Laeng et al.*, 2014].

The effects of the SPEs on observed ozone are evident in Figure 6. The observed amount of ozone decreases by 35–50% above 55 km after SPE1 and by up to 60% above 74 km after SPE2. In the middle mesosphere, above about 60 km, ozone starts to return back to the pre-SPE levels after SPE2, maximizing by the beginning of February. In the model, the timing of the ozone loss in connection to the SPEs is correct, but the magnitude of the absolute loss differs by 70–80%. Of course, the background level of the simulated ozone was lower already in the beginning, and therefore, all changes in ozone appear to be larger, at least farther away from the upper boundary. The vicinity of the upper boundary (MLS climatology) affects the altitudes above 75 km, possibly explaining at least some of the ozone differences in the upper mesosphere. However, the behavior of ozone in the middle mesosphere after SPE2, i.e., the increase in ozone back to the SPE preceding levels, is reproduced also by the model. Clear ozone losses are also observed after SPE3. The event has an effect even down to about 48 km with ozone decreasing by ∼10–40%, whereas SPE4 seems to have effect only above about 72 km, i.e., close to the upper limit of the observations, with ozone losses of up to 90%. For SPE4, the simulation and observations differ by 10–90% both in the middle and upper mesosphere.

Figure 7 shows time series of the observed and modeled ozone in the upper stratosphere (46 km) and lower mesosphere (60 km), similar to Figure 4 presented earlier. Due to the clearly lower absolute values of ozone in the model, we have multiplied the results with a factor of 4 and 2 in the stratosphere and mesosphere, respectively, in order to aid the comparison of variability. The general variability in ozone during January to

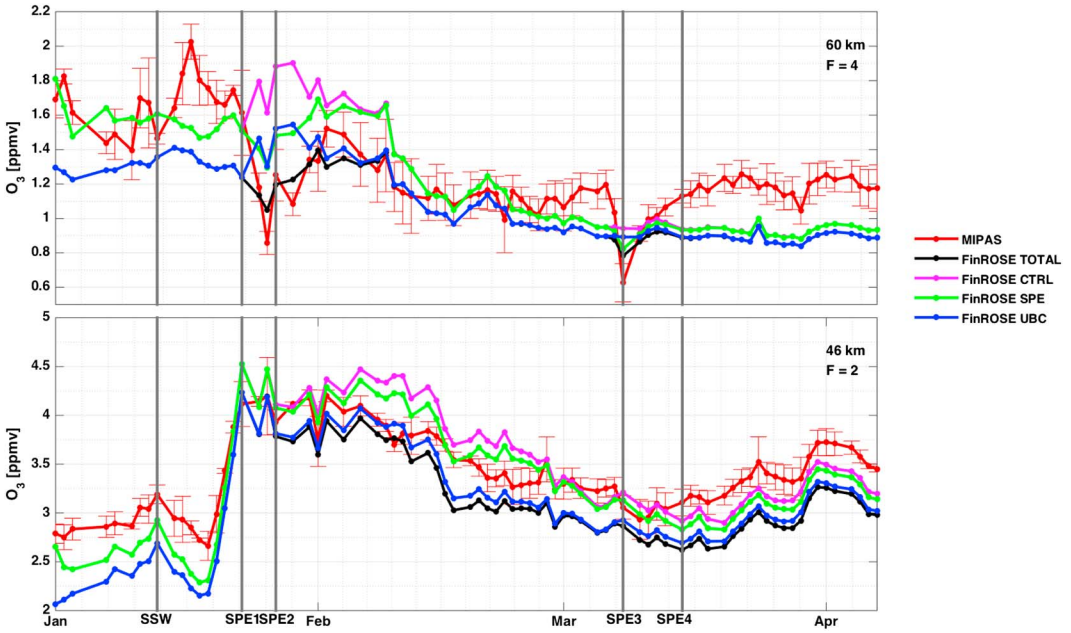

Figure 7. Same as Figure 4 but for ozone. The absolute values of the modeled ozone are multiplied with a factor of 4 ($F=4$) and 2 ($F=2$) in the mesosphere and stratosphere, respectively, in order to aid the comparison with the observed values.

early April is very similar in the model results and in the observations, although the absolute values differ greatly. However, only the all-encompassing and SPE run are able to reproduce the ozone depletion due to radicals such as NO_x and HO_x, the effect being stronger in the mesosphere. The NO_y UBC applied in the UBC and all-encompassing runs decrease the absolute values of ozone during the whole period of interest.

According to the model-observation comparison, the model performance seems to be in a reasonable agreement with the observations. This gives us a good basis for analyzing the separate contributions of transport and in situ forcing on the stratospheric NO_x and ozone. However, the comparison revealed also differences that might affect the contribution analysis to some extent. The downward transport of NO_x after the SSW in mid-January was stronger in the simulation and led up to 135% higher NO_x amounts during the most intense descent above about 40 km, possibly leading to an overestimation of the respective ozone loss in the stratosphere. Differences of up to 110% took place also after the SPEs in the mesosphere, but the agreement (~20%) in the stratosphere was reasonably good. The simulated amount of ozone in the stratosphere was lower down to ~33 km, and NO_x produced ozone losses above this level may thus be overestimated since the model is sensitive to even quite small changes. Due to the stronger NO_x descent from the MLT down to the stratosphere and the lower ozone amounts in the same region in the simulations, the contribution analysis should be considered to represent the maximum changes in both NO_x and ozone in the middle atmosphere.

5. Contributions of Transport and In Situ Forcing

Figure 8 shows NO_x in the control run, averaged over 70–90°N, and the changes due to UBC and SPEs (applied separately and together in runs 2–4) compared to the control run. The largest effect in the mesosphere, above about 50 km, arises from the implementation of the UBC (shown also in Figure 4). Changes of the order of 4–80 ppbv between 50 and 70 km are visible already from the beginning of the year due to descent of MLT NO_x inside the polar vortex (not seen by MIPAS, see section 4). The descent was interrupted by the mid-January SSW but continued again after reformation of the polar vortex shortly after the SSW. Between 70 and 80 km NO_x increases by 35–650 ppbv in early to mid-January, propagating with elevated levels down to about 50 km after the SSW in mid-January. Strongest descent of NO_x lasts until the end of March bringing 4–7 ppbv (100–300%) more NO_x down to even 45 km, although signs of increased NO_x are visible still in late April.

The mesospheric effects of the January/March SPEs on NO_x maximize during the events with magnitudes of even 36 ppbv above 60 km. The enhanced NO_x is transported downward inside the polar vortex so that the effects of the January SPEs are visible only about 2 weeks above 60 km with NO_x increases of 0.1–36 ppbv but

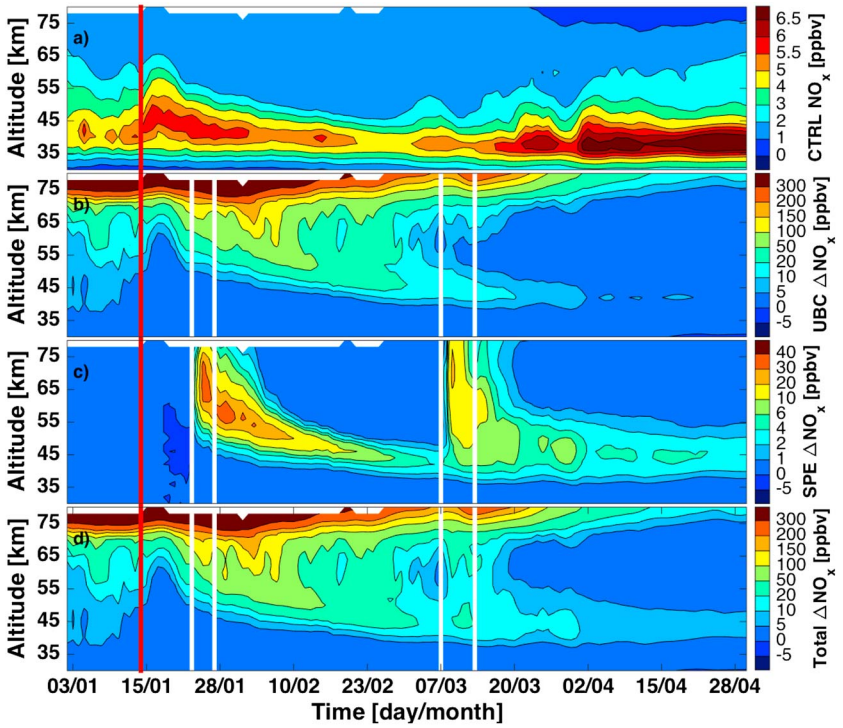

Figure 8. FinROSE NO_x results in January–April 2012. (a) Run 1 (control). (b) Difference between the UBC and control runs. (c) Difference between the SPE and control runs. (d) Difference between the all-encompassing (UBC + SPE) and control runs. White lines indicate the time points of the SPEs and the red solid line the SSW.

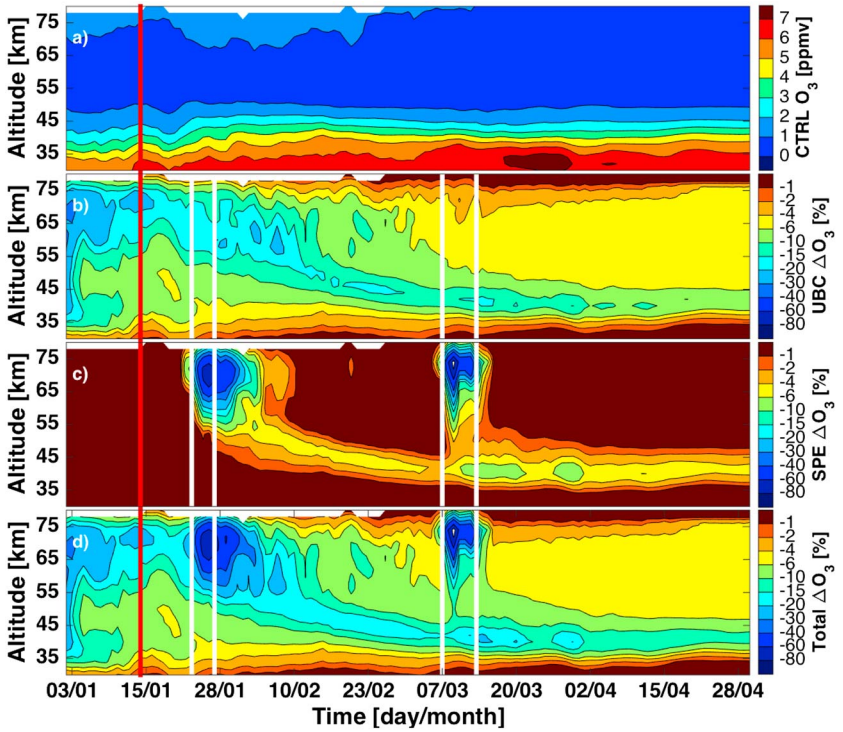

Figure 9. Same as Figure 8 but for ozone.

Table 2. Maximum Ozone Loss (%) After Sudden Stratospheric Warming and Solar Proton Events in Early 2012[a]

	30–50 km (%)	50–60 km (%)	60–75 km (%)
SPE	9	22	87
UBC	17	24	24

[a]Changes are calculated separately for the SPE (all events included) and UBC effects for the given altitude ranges in the stratosphere and mesosphere.

remain even longer than 1 month below 60 km with same order of magnitude increases. The March SPEs have a more constant effect on NO_x in the vertical direction due to the already weakened downward transport after the SSW in January. Above 50 km NO_x increases by 0.1–22 ppbv after SPE3, and the effect seems to remain from 1 to 2 months at upper to lower mesospheric altitudes, respectively. SPE4 increases the amounts only between 53 and 67 km by 0.2–15 ppbv.

In the stratosphere, below about 50 km, NO_x descends down to about 36 km with mixing ratios of ~1.3 ppbv by early March, indicating an increase of at least about 30% only due to the implementation of the UBC. Just at and below the stratopause region the changes are maximizing with NO_x increases up to 60 ppbv between early and late February. When analyzing the SPE run, it is clear that the in situ production, taken into account at all stratospheric altitudes, causes NO_x to increase by up to 21 ppbv after the January and 14 ppbv after the March SPEs. The effect of the January SPEs descends down to about 35 km by SPE3, after which the effect can be seen as low as 33 km altitude. The NO_x increase after the March SPEs does not descend much lower in the stratosphere, but the effect stays visible until the end of April.

Figure 9 shows the corresponding changes in ozone. The UBC effect on mesospheric ozone is visible already in the beginning of January with ozone losses of 30–40%, coinciding with the enhanced amounts of NO_x in the model. After the mid-January SSW, ozone losses are around 15–20% during the most intense NO_x descent but recover by about 10% by early March. The stratospheric ozone changes are less pronounced compared to those in the mesosphere: the implementation of the UBC, and the following downward transport of NO_x, causes ozone to decrease by up to ~30% in January before the SSW and up to ~15% after the SSW from 30 to 50 km.

Contrary to the NO_x enhancements, which are largely due to descent, the most substantial ozone decrease in the mesosphere is caused by the SPEs. The decrease is clear throughout the whole mesosphere during and shortly after (from days to couple of weeks) the SPEs, maximizing around 70 km with ozone losses up to ~90%. According to previous studies of the effects of different SPEs in the middle and upper atmosphere [e.g., *Verronen et al.*, 2006], the in situ mesospheric ozone losses during the SPEs are mainly caused by the increased HO_x production in the same region. Note that FinROSE ozone response is in agreement with the results presented for the same SPEs by *Jackman et al.* [2014].

Between 50 and 60 km, up to ~20% ozone loss is still visible 1–4 weeks after the SPEs due to downward transport of the SPE produced NO_x. The altitude range (30–50 km) for the stratospheric ozone changes is very similar for both UBC and SPE cases. However, in this region, the SPE effects on ozone are about a factor of 2 smaller compared to the UBC effects, and the model suggests ozone losses of up to about 10% after the January/March SPEs. Ozone changes due to the indirect UBC effect (NO_x downward transport) and SPE effect at different mesospheric and stratospheric altitudes, calculated from the SPE and UBC runs, are presented in more detail in Table 2.

6. Discussion

Päivärinta et al. [2013] showed that both short-term and long-term ozone changes were observed in early 2012 after intensified NO_x descent from MLT down to the stratosphere, following a SSW in mid-January, and in situ production of NO_x due to several SPEs in January/March. They concluded that the short-term (few days) ozone losses in the mesosphere were driven by HO_x chemistry, but they could not separate the effects of transport and SPEs on the longer-term (weeks) ozone depletion in the mesosphere and upper stratosphere by using only satellite observations. Our model results show that the indirect UBC effect brings much larger NO_x amounts (7–48 ppbv) below the stratopause level than the SPE effect (<21 ppbv) for these particular events.

The enhanced NO_x in the stratosphere, in turn, further affects the stratospheric ozone levels. According to the model, the indirect UBC effect on ozone is double (see Table 2) compared to the SPE effect, directly connected to the NO_x amounts in the stratosphere.

An interesting feature in the model results is the middle mesospheric ozone decrease (e.g., 30–40% at 65–75 km in early January) caused by the NO_y UBC forcing (Figure 9). The same effect is also seen in the all-encompassing run before the January SPEs as well as between the January and March SPEs. The NO_x catalytic cycles depleting ozone are not important in mesosphere [e.g., *Grenfell et al.*, 2006]. Thus, the ozone decrease seems to be related to changes in the HO_x nighttime partitioning and loss caused by the NO_x enhancement, which lead to increase in the daytime HO_x amount and ozone loss rates [*Verronen and Lehmann*, 2015]. Indeed, comparing the UBC and control runs, we find that the nighttime HO_x partitioning changes below 75 km (not shown). As seen in Figure 9, this leads to a longer-term effect on ozone lasting from early January to mid-February, contrary to the short-term (but larger) effect caused by the direct HO_x increase during SPEs. The stronger ozone effect in January, compared to February when the model actually shows larger NO_x amounts, is due to the enhanced amounts of NO_x strongly affecting ozone already in late 2011 (not shown). NO_x decreases from the December values in January due to polar vortex dynamics, which leads to ozone recovery in early January (Figure 9). However, this recovery is relatively slow, and thus, the January ozone depletion is higher than what is seen in February. Also, the HO_x partitioning effect caused by high NO_x is relatively stronger in January than in February (not shown).

Funke et al. [2011] reported the effects of the 2003 October/November SPEs on the middle and upper atmosphere composition by using both observations and several atmospheric models, including the FinROSE-CTM. They concluded that models using an incomplete SPE parameterization in order to reproduce the observed HNO_3 increases seem to, in general, underestimate the HNO_3 amounts considerably. The new and revised parameterization used in this study shows significant improvement in reproducing of HNO_3 observations during the SPEs. Although the model somewhat overestimates the amount of HNO_3 when contrasted to the observations (a factor of <2.7 in January and <1.4 in March), the simulated results are clearly in reasonable agreement with the observed magnitude and altitude extent of the enhancements. MLS errors (standard error of the mean) grow up to 60% and 100% above 45 km during the January (SPE1 and SPE2) and March (SPE3) events, respectively, possibly explaining part of the differences. Note that uncertainties in the parameterization of HNO_3-producing ion chemistry are not the main reason for the model overestimation during SPE1 (in fact, during all other SPEs the modeled values are in much better agreement with the observations). First, understanding of the ionic reactions and rates affecting HNO_3 is satisfactory [*Verronen et al.*, 2011]. Second, although the parameterized HNO_3 production factors used here have additional uncertainty due to assumptions made on atmospheric composition when deriving them, according to *Verronen and Lehmann* [2013], this should be of the order of 24%. Instead, the FinROSE-MIPAS differences are better explained by relatively large measurement uncertainty (as mentioned above), and uncertainties of the reanalysis data (temperature, winds, and total density) used in the model (see final paragraph of this section). The reanalysis data are important here because they drive polar vortex dynamics that have been shown to have a strong effect on the day-to-day distribution of SPE-produced HNO_3 [*Verronen et al.*, 2011].

Note that the early 2012 SPEs took place during a rather weak solar maximum, and the background MLT NO_x production by energetic particles was low. Relatively low amounts of NO_x were transported down to the stratosphere, and although combined with the small to medium-strength SPEs, a clear NO_x-dominated impact on stratospheric ozone was not observed [*Päivärinta et al.*, 2013]. The FinROSE results do, however, show that the transport from MLT to lower atmosphere plays a very important role in the stratospheric NO_x-ozone connection, even on a time scale of weeks to months.

The results of the contribution analysis in this study are based on CTM results only. Although the model performs reasonably well when compared to observations, the results have to be considered as an estimation. As already mentioned in section 4, the too strong NO_x descent from MLT down to the stratosphere in FinROSE, and lower ozone amounts in the same region, indicates that our results could overemphasize the transport effect during periods of intensified descent. Nevertheless, the overlapping timing of the different events at this time provided us with an opportunity to utilize an atmospheric model to separate the roles of in situ (i.e., SPE) and transport effects on middle atmospheric composition. This is not straightforward with most satellite observations. The meteorological input for the CTM is reanalysis data, i.e., produced by numerical models, and thus a source for uncertainty, even though they are based on assimilating observations into the

models. Differences in various reanalysis data have been discussed by, e.g., *Martineau and Son* [2010] and *Lawrence et al.* [2015]. In fact, some further testing (not shown) suggests that using another reanalysis data set leads to a different vertical and horizontal distribution of the simulated species, e.g., through changes in the descent rates, although the main features of the SPE effect and indirect UBC effect still remain the same. However, the differing dynamical variables seem to lead to, e.g., lower modeled HNO_3 amounts during the January/March SPE periods. A detailed analysis of the impact of changing the meteorological input in the CTM is beyond the scope of this paper and a topic of a future study. Yet this emphasizes the real need of reliable meteorological input data for atmospheric models in order to reproduce the observed fields as well as possible but also the need of continuous satellite observations in the stratosphere and MLT region to be used in both assimilation processes and validating the models.

7. Conclusions

We have assessed the relative contributions of indirect and direct effects on the stratospheric NO_x and ozone in the Northern polar cap area (70–90°), using a CTM with an UBC for the NO_y species and an improved parameterization scheme for the early 2012 SPEs. The results show that the amount of NO_x increased due to both effects, but more pronounced stratospheric impact, was caused by the intensified downward transport of NO_x after the mid-January SSW. The model suggests NO_x enhancements of up to 3300% (<48 ppbv) just below the stratopause level (~50 km), and even up to 120% (5 ppbv) as low as 38 km altitude. The SPE effect on NO_x was visible at the same stratospheric altitudes as increased NO_x amounts of up to 1200% (<21 ppbv) above 35 km and up to 820% (<14 ppbv) above 33 km were simulated after the January and March SPEs, respectively. The following effect on the stratospheric ozone was greater for the indirect UBC effect, leading to ozone losses of up to 17%, whereas the SPE effect caused ozone losses of 9%.

Although the conditions in early 2012 were not ideal, due to the small/medium magnitude of the SPEs and low background production of NO_x in the MLT region, stratospheric signal on both NO_x and ozone was still evident in both cases. This emphasizes the importance of both middle atmosphere dynamics and the geomagnetic activity on the chemical composition of the stratosphere, possibly propagating farther down into the troposphere. Continuation of middle atmosphere observations and high-quality reanalysis data is needed in order to investigate the MLT-stratosphere connection also during periods of high solar activity when the combination of optimal dynamics (i.e., intensified downward transport following SSWs), and EPP is likely to have even greater impact in the stratosphere.

Acknowledgments

The work of S.M.P., P.T.V., A.S., and M.E.A. was supported by the Academy of Finland through the projects 276926 (SECTIC: Sun-Earth Connection Through Ion Chemistry), 258165, and 265005 (CLASP: Climate and Solar Particle Forcing). The work of B.F. and A.G. was supported by the Spanish MCINN under grant AYA2011-23552 and EC FEDER funds. MIPAS/Envisat and MLS/Aura data are provided by European Space Agency (ESA) and National Aeronautics and Space Administration (NASA), respectively. The FinROSE data supporting the analysis and conclusions have been archived and are available upon request from the corresponding author.

References

Andrews, D. G., J. R. Holton, and C. B. Leovy (1987), *Middle Atmosphere Dynamics*, pp. 259–260, Academic Press, New York.

Barth, C. A. (1992), Nitric oxide in the lower thermosphere, *Planet. Space Sci.*, *40*, 315–336.

Baumgaertner, A. J. G., A. Seppälä, P. Jöckel, and M. A. Clilverd (2011), Geomagnetic activity related NO_x enhancements and polar surface air temperature variability in a chemistry climate model: Modulation of the NAM index, *Atmos. Chem. Phys.*, *11*, 4521–4531, doi:10.5194/acp-11-4521-2011.

Callis, L. B., D. N. Baker, J. B. Blake, J. D. Lambeth, R. E. Boughner, M. Natarajan, R. W. Klebesadel, and D. J. Gorney (1991), Precipitating relativistic electrons: Their long-term effect on stratospheric odd nitrogen levels, *J. Geophys. Res.*, *96*, 2939–2976.

Charlton, A. J., and L. M. Polvani (2007), A new look at stratospheric sudden warmings. Part I: Climatology and modeling benchmarks, *J. Clim.*, *20*, 449–469, doi:10.1175/JCLI3996.1.

Clilverd, M. A., A. Seppälä, C. J. Rodger, P. T. Verronen, and N. R. Thomson (2006), Ionospheric evidence of thermosphere-to-stratosphere descent of polar NO_x, *Geophys. Res. Lett.*, *33*, L19811, doi:10.1029/2006GL026727.

Clilverd, M. A., A. Seppälä, C. J. Rodger, M. G. Mlynczak, and J. U. Kozyra (2009), Additional stratospheric NO_x production by relativistic electron precipitation during the 2004 spring NO_x descent event, *J. Geophys. Res.*, *114*, A04305, doi:10.1029/2008JA013472.

Damiani, A., M. Storini, M. L. Santee, and S. Wang (2010), Variability of the nighttime OH layer and mesospheric ozone at high latitudes during northern winter: Influence of meteorology, *Atmos. Chem. Phys.*, *10*, 10,291–10,303, doi:10.5194/acp-10-10291-2010.

Damski, J., L. Thölix, L. Backman, J. Kaurola, P. Taalas, J. Austin, N. Butchart, and M. Kulmala (2007), A chemistry-transport model simulation of middle atmospheric ozone from 1980 to 2019 using coupled chemistry GCM winds and temperatures, *Atmos. Chem. Phys.*, *7*, 2165–2181.

Funke, B., et al. (2011), Composition changes after the "Halloween" solar proton event: The High-Energy Particle Precipitation in the Atmosphere (HEPPA) model versus MIPAS data intercomparison study, *Atmos. Chem. Phys.*, *11*, 9089–9139, doi:10.5194/acp-11-9089-2011.

Funke, B., M. López-Puertas, G. P. Stiller, and T. von Clarmann (2014a), Mesospheric and stratospheric NO_y produced by energetic particle precipitation during 2002–2012, *J. Geophys. Res. Atmos.*, *119*, 4429–4446, doi:10.1002/2013JD021404.

Funke, B., M. López-Puertas, L. Holt, C. E. Randall, G. P. Stiller, and T. von Clarmann (2014b), Hemispheric distributions and interannual variability of NO_y produced by energetic particle precipitation in 2002–2012, *J. Geophys. Res. Atmos.*, *119*, 13,565–13,582, doi:10.1002/2014JD022423.

Grenfell, J. L., R. Lehmann, P. Mieth, U. Langematz, and B. Steil (2006), Chemical reaction pathways affecting stratospheric and mesospheric ozone, *J. Geophys. Res.*, *111*, D17311, doi:10.1029/2004JD005713.

Holt, L. A., C. E. Randall, E. D. Peck, D. R. Marsh, A. K. Smith, and V. L. Harvey (2013), The influence of major sudden stratospheric warming and elevated stratopause events on the effects of energetic particle precipitation in waccm, *J. Geophys. Res. Atmos.*, *118*, 11,636–11,646, doi:10.1002/2013JD020294.

Jackman, C. H., M. T. DeLand, G. J. Labow, E. L. Fleming, D. K. Weisenstein, M. K. W. Ko, M. Sinnhuber, and J. M. Russell (2005), Neutral atmospheric influences of the solar proton events in October–November 2003, *J. Geophys. Res.*, *110*, A09S27, doi:10.1029/2004JA010888.

Jackman, C. H., et al. (2008), Short- and medium-term atmospheric constituent effects of very large solar proton events, *Atmos. Chem. Phys.*, *8*, 765–785, doi:10.5194/acp-8-765-2008.

Jackman, C. H., D. R. Marsh, F. M. Vitt, R. R. Garcia, C. E. Randall, E. L. Fleming, and S. M. Frith (2009), Long-term middle atmospheric influence of very large solar proton events, *J. Geophys. Res.*, *114*, D11304, doi:10.1029/2008JD011415.

Jackman, C. H., C. E. Randall, V. L. Harvey, S. Wang, E. L. Fleming, M. López-Puertas, B. Funke, and P. F. Bernath (2014), Middle atmospheric changes caused by the January and March 2012 solar proton events, *Atmos. Chem. Phys.*, *14*, 1025–1038, doi:10.5194/acp-14-1025-2014.

Kvissel, O.-K., Y. J. Orsolini, F. Stordal, I. S. A. Isaksen, and M. L. Santee (2012), Formation of stratospheric nitric acid by a hydrated ion cluster reaction: Implications for the effect of energetic particle precipitation on the middle atmosphere, *J. Geophys. Res.*, *117*, D16301, doi:10.1029/2011JD017257.

Kylling, A., A. Albold, and G. Seckmeyer (1997), Transmittance of a cloud is wavelength—Dependent in the UV-range: Physical interpretation, *Geophys. Res. Lett.*, *24*(4), 397–400, doi:10.1029/97GL00111.

Laeng, A., et al. (2014), Validation of MIPAS IMK/IAA V5R_O3_224 ozone profiles, *Atmos. Meas. Tech.*, *7*(11), 3971–3987, doi:10.5194/amt-7-3971-2014.

Langematz, U., M. Kunze, K. Kruger, K. Labitzke, and G. L. Roff (2003), Thermal and dynamical changes of the stratosphere since 1979 and their link to ozone and CO_2 changes, *J. Geophys. Res.*, *104*(D1), 4027, doi:10.1029/2002JD002069.

Lawrence, Z. D., G. L. Manney, K. Minschwaner, M. L. Santee, and A. Lambert (2015), Comparisons of polar processing diagnostics from 34 years of the ERA-Interim and MERRA reanalyses, *Atmos. Chem. Phys.*, *15*, 3873–3892, doi:10.5194/acp-15-3873-2015.

Limpasuvan, V., J. H. Richter, Y. J. Orsolini, F. Stordal, and O.-K. Kvissel (2012), The roles of planetray and gravity waves during a major stratospheric sudden warming as characterized in WACCM, *J. Atmos. Sol. Terr. Phys.*, *78–79*, 84–98, doi:10.1016/j.jastp.2011.03.004.

Livesey, N. J., et al. (2015), EOS MLS Version 4.2x Level 2 data quality and description document, *JPL D-33509*, Jet Propul. Lab., California Inst. Technol., Pasadena, Calif.

López-Puertas, M., B. Funke, S. Gil-López, T. von Clarmann, G. P. Stiller, M. Höpfner, S. Kellmann, H. Fischer, and C. H. Jackman (2005), Observation of NO_x enhancement and ozone depletion in the Northern and Southern Hemispheres after the October–November 2003 solar proton events, *J. Geophys. Res.*, *110*, A09S43, doi:10.1029/2005JA011050.

Lu, H., M. J. Jarvis, and R. Hibbins (2008), Possible solar wind effect on the northern annular mode and Northern Hemispheric circulation during winter and spring, *J. Geophys. Res.*, *113*, D23104, doi:10.1029/2008JD010848.

Manney, G. L., et al. (2008), The evolution of the stratopause during the 2006 major warming: Satellite data and assimilated meteorological analyses, *J. Geophys. Res.*, *113*, D11115, doi:10.1029/2007JD009097.

Manney, G. L., M. J. Schwartz, K. Krüger, M. L. Santee, S. Pawson, J. N. Lee, W. H. Daffer, R. A. Fuller, and N. J. Livesey (2009), Aura Microwave Limb Sounder observations of dynamics and transport during the record-breaking 2009 Arctic stratospheric major warming, *Geophys. Res. Lett.*, *36*, L12815, doi:10.1029/2009GL038586.

Martineau, P., and S.-W. Son (2010), Quality of reanalysis data during stratospheric vortex weakening and intensification events, *Geophys. Res. Lett.*, *37*, L22801, doi:10.1029/2010GL045237.

Matsuno, T. (1971), A dynamical model of the sudden stratospheric warming, *J. Atmos. Sci.*, *28*, 1479–1494.

Newman, P. A., and E. R. Nash (2005), The unusual Southern Hemisphere stratosphere winter of 2002, *J. Atmos. Sci*, *62*, 614–628, doi:10.1175/JAS-3323.1.

Orsolini, Y. J., J. Urban, D. P. Murtagh, S. Lossow, and V. Limpasuvan (2010), Descent from the polar mesosphere and anomalously high stratopause observed in 8 years of water vapor and temperature satellite observations by the odin sub-millimeter radiometer, *J. Geophys. Res.*, *115*, D12305, doi:10.1029/2009JD013501.

Päivärinta, S.-M., A. SeppäLä, M. E. Andersson, P. T. Verronen, L. ThöLix, and E. KyröLä (2013), Observed effects of solar proton events and sudden stratospheric warmings on odd nitrogen and ozone in the polar middle atmosphere, *J. Geophys. Res. Atmos.*, *118*, 6837–6848, doi:10.1002/jgrd.50486.

Randall, C. E., et al. (2005), Stratospheric effects of energetic particle precipitation in 2003–2004, *Geophys. Res. Lett.*, *32*, L05802, doi:10.1029/2004GL022003.

Randall, C. E., V. L. Harvey, D. E. Siskind, J. France, P. F. Bernath, C. D. Boone, and K. A. Walker (2009), NO_x descent in the Arctic middle atmosphere in early 2009, *Geophys. Res. Lett.*, *36*, L18811, doi:10.1029/2009GL039706.

Rienecker, M. M., et al. (2011), MERRA: NASA's modern-era retrospective analysis for research and applications, *J. Clim.*, *24*, 3624–3648, doi:10.1175/JCLI-D-11-00015.1.

Rozanov, E., L. Callis, M. Schlesinger, F. Yang, N. Andronova, and V. Zubov (2005), Atmospheric response to NO_y source due to energetic electron precipitation, *Geophys. Res. Lett.*, *32*, L14811, doi:10.1029/2005GL023041.

Rozanov, E., M. Calisto, T. Egorova, T. Peter, and W. Schmutz (2012), The influence of precipitating energetic particles on atmospheric chemistry and climate, *Surv. Geophys.*, *33*, 483–501, doi:10.1007/s10712-012-9192-0.

Salmi, S.-M., P. T. Verronen, L. Thölix, E. Kyrölä, L. Backman, A. Y. Karpechko, and A. Seppälä (2011), Mesosphere-to-stratosphere descent of odd nitrogen in February–March 2009 after sudden stratospheric warming, *Atmos. Chem. Phys.*, *11*, 4645–4655, doi:10.5194/acp-11-4645-2011.

Sander, S. P., et al. (2006), Chemical kinetics and photochemical data for use in atmospheric studies, *Eval. Num. 15, JPL Publ. 06-2*, Jet Propulsion Lab., Calif. Inst. of Tech., Pasadena, Calif.

Santee, M. L., et al. (2007), Validation of the aura microwave limb sounder HNO_3 measurements, *J. Geophys. Res.*, *112*, D24S40, doi:10.1029/2007JD008721.

Semeniuk, K., J. C. McConnell, and C. H. Jackman (2005), Simulation of the October–November 2003 solar proton events in the CMAM GCM: Comparison with observations, *Geophys. Res. Lett.*, *32*, L15S02, doi:10.1029/2005GL022392.

Seppälä, A., P. T. Verronen, E. Kyrölä, S. Hassinen, L. Backman, A. Hauchecorne, J. L. Bertaux, and D. Fussen (2004), Solar proton events of October–November 2003: Ozone depletion in the Northern Hemisphere polar winter as seen by GOMOS/Envisat, *Geophys. Res. Lett.*, *31*, L19107, doi:10.1029/2004GL021042.

Seppälä, A., M. A. Clilverd, C. J. Rodger, P. T. Verronen, and E. Turunen (2008), The effects of hard-spectra solar proton events on the middle atmosphere, *J. Geophys. Res.*, *113*, A11311, doi:10.1029/2008JA013517.

Seppälä, A., H. Lu, M. A. Clilverd, and C. J. Rodger (2013), Geomagnetic activity signatures in wintertime stratosphere wind, temperature, and wave response, *J. Geophys. Res. Atmos.*, *118*, 2169–2183, doi:10.1002/jgrd.50236.

Smith, A. K. (1995), Numerical simulation of global variations of temperature, ozone, and trace species in the stratosphere, *J. Geophys. Res.*, *100*, 1253–1269, doi:10.1029/94JD02395.

Smith, A. K., M. López-Puertas, M. García-Comas, and S. Tukiainen (2009), SABER observations of mesospheric ozone during NH late winter 2002–2009, *Geophys. Res. Lett.*, *36*, L23804, doi:10.1029/2009GL040942.

Sofieva, V. F., N. Kalakoski, P. T. Verronen, S.-M. Päivärinta, E. Kyrölä, L. Backman, and J. Tamminen (2012), Polar-night O_3, NO_2 and NO_3 distributions during sudden stratospheric warmings in 2003–2008 as seen by GOMOS/Envisat, *Atmos. Chem. Phys.*, *12*, 1051–1066, doi:10.5194/acp-12-1051-2012.

Solomon, S., P. J. Crutzen, and R. G. Roble (1982), Photochemical coupling between the thermosphere and the lower atmosphere 1. Odd nitrogen from 50 to 120 km, *J. Geophys. Res.*, *87*, 7206–7220.

Thompson, D. W. J., M. P. Baldwin, and S. Solomon (2005), Stratospher–troposphere coupling in the Southern Hemisphere, *J. Atmos. Sci.*, *62*, 708–715, doi:10.1175/JAS-3321.1.

Verronen, P. T., and R. Lehmann (2013), Analysis and parameterisation of ionic reactions affecting middle atmospheric HO_x and NO_y during solar proton events, *Ann. Geophys.*, *31*, 909–956, doi:10.5194/angeo-31-909-2013.

Verronen, P. T., and R. Lehmann (2015), Enhancement of odd nitrogen modifies mesospheric ozone chemistry during polar winter, *Geophys. Res. Lett.*, *42*, 10,445–10,452, doi:10.1002/2015GL066703.

Verronen, P. T., A. Seppälä, M. A. Clilverd, C. J. Rodger, E. Kyrölä, C.-F. Enell, T. Ulich, and E. Turunen (2005), Diurnal variation of ozone depletion during the October–November 2003 solar proton events, *J. Geophys. Res.*, *110*, A09S32, doi:10.1029/2004JA010932.

Verronen, P. T., A. Seppälä, E. Kyrölä, J. Tamminen, H. M. Pickett, and E. Turunen (2006), Production of odd hydrogen in the mesosphere during the January 2005 solar proton event, *Geophys. Res. Lett.*, *33*, L24811, doi:10.1029/2006GL028115.

Verronen, P. T., M. L. Santee, G. L. Manney, R. Lehmann, S.-M. Salmi, and A. Seppälä (2011), Nitric acid enhancements in the mesosphere during the January 2005 and December 2006 solar proton events, *J. Geophys. Res.*, *116*, D17301, doi:10.1029/2011JD016075.

von Clarmann, T., B. Funke, M. López-Puertas, S. Kellmann, A. Linden, G. P. Stiller, C. H. Jackman, and V. L. Harvey (2013), The solar proton events in 2012 as observed by MIPAS, *Geophys. Res. Lett.*, *40*, 2339–2343, doi:10.1002/grl.50119.

Waters, J. W., et al. (2006), The Earth Observing System Microwave Limb Sounder (EOS MLS) on the Aura satellite, *IEEE Trans. Geosci. Remote Sens.*, *44*, 1075–1092, doi:10.1109/TGRS.2006.873771.